Electrochimica Acta 105 (2013) 535–541

Contents lists available at SciVerse ScienceDirect

Electrochimica Acta

journal homepage: www.elsevier.com/locate/electacta

Preparation of CdS NCs decorated TiO_2 nano-tubes arrays photoelectrode and its enhanced photoelectrocatalytic performance and mechanism

Xiuwen Cheng[c], Guoping Pan[b], Xiujuan Yu[a,b,*], Tong Zheng[c]

[a] Key Laboratory of Chemical Engineering Process & Technology for High-Efficiency Conversion, College of Heilongjiang Province, Xuefu Road 74, Nangang District, Harbin 150080, PR China
[b] Department of Environmental Science and Engineering, Heilongjiang University, Xuefu Road 74, Nangang District, Harbin 150080, PR China
[c] State Key Laboratory of Urban Water Resources and Environment (SKLUWRE), Department of Environmental Science and Engineering, Harbin Institute of Technology, Huanghe Road 73, Nangang District, Harbin 150090, PR China

ARTICLE INFO

Article history:
Received 22 February 2013
Received in revised form 30 April 2013
Accepted 14 May 2013
Available online 21 May 2013

Keywords:
CdS NCs/TiO_2 NTAs
Photoelectrode
Photoelectrocatalysis
Electrodeposition
RhB

ABSTRACT

CdS nano-crystallites decorated TiO_2 nano-tubes arrays (CdS NCs/TiO_2 NTAs) photoelectrodes were prepared through anodization, followed by electrodeposition strategy. Subsequently, structures of the resulting CdS NCs/TiO_2 NTAs samples were characterized by scanning electron microscopy (SEM), transmission electron microscopy (TEM) and X-ray diffraction (XRD). In addition, the light absorption capacities and photoelectrochemical (PECH) properties were investigated through UV–visible diffuse reflectance spectrum (DRS), photocurrent response (PCR) and open-circuit photovoltage (OCP). Furthermore, photodecomposition performances were evaluated by the yield of •OH radicals and photoelectrocatalytic (PEC) degradation of rhodamine B (RhB) under Xenon light irradiation. Moreover, the enhanced PC mechanism was proposed and confirmed through photoluminescence (PL) spectra and contribution of different reactive species. Results showed that hexagonal CdS NCs with uniform spherical sizes of 20 nm were successfully deposited onto the surface of highly ordered TiO_2 NTAs, which could not only red-shift the light absorption to visible region between 400 and 700 nm, but also significantly enhance the generation of •OH radicals. Furthermore, CdS NCs/TiO_2 NTAs photoelectrodes possessed higher transient photogenerated current of 9.62 mA cm^{-2} and open-circuit photovoltage of −0.253 V cm^{-2} than that of bare TiO_2 NTAs. Moreover, when external potential (−2 V) was applied, CdS NCs/TiO_2 TNTAs samples performed higher PEC efficiency of 91.6%, which could be attributed to the intense light harvesting in visible region and high mobility and separation efficiency of photogenerated charge carriers.

1. Introduction

With the development of modern society, environmental pollutants and energy crisis have been considered as two urgent issues. Semiconductor-based photocatalytic (PC) technique has been developed as one of potential strategies to solve the above problems, including solar energy conversion, air purification and waste water treatment [1–3]. Among these semiconductors, titanium dioxide (TiO_2) has been widely studied due to its exceptional properties such as low cost, non-toxicity, chemical stability and outstanding oxidization ability. However, the application of TiO_2 nano-materials was greatly restricted due to its intrinsic defects. Firstly, pure TiO_2 can only be excited by UV light, which only occupied 5% of the solar spectrum [4]. Secondly, pulverous TiO_2 was difficult to separate and recover in the suspending system. Thirdly, high recombination rate of photogenerated charge carriers lowered the PC efficiency. Thus, to conquer these drawbacks, a great deal of efforts has been conducted.

Recently, one-dimensional (1D) nano-architectures, such as TiO_2 nano-tube (NTs), have been demonstrated as a versatile candidate for the improvement of PC performance because of the exceptional charge transport and light-harvest properties [5]. Besides these, the direct growth of TiO_2 NTs onto the Ti substrate greatly improved the recycle of the catalyst. From then on, numerous of studies have been carried out.

Very recently, TiO_2 decorated with a narrower material has been demonstrated as an effective strategy to improve the visible light PC performance, because the narrower semiconductor could

* Corresponding author at: Department of Environmental Science and Engineering, Heilongjiang University, Xuefu Road 74, Nangang District, Harbin 150080, PR China. Tel.: +86 451 86608549; fax: +86 451 86413259.
E-mail address: yuxjuan@hit.edu.cn (X. Yu).

0013-4686/$ – see front matter © 2013 Elsevier Ltd. All rights reserved.
http://dx.doi.org/10.1016/j.electacta.2013.05.040

absorb more photons to participate in the PC reaction [6,7]. In addition, the higher mobility and separation of photogenerated charge carriers could induce a higher PC efficiency. Among which, CdS nano-material have been received more focus [8–10].

Although there were many reports about the synthesis of CdS decorated TiO_2 composite catalysts. However, these reports were mainly related with the pulverous CdS/TiO_2 composites. To the best of our knowledge, it was still lack of comprehensive investigation about the preparation of CdS NCs decorated TiO_2 NTAs and its enhanced PC mechanism. Thus, in the present study, CdS nano-crystallite decorated TiO_2 NTAs (CdS NCs/TiO_2 NTAs) photoelectrodes have been prepared through anodization method, followed by electrodeposition strategy. Furthermore, the enhanced photoelectrocatalytic (PEC) performance and mechanism were discussed in detail. As a result, CdS NCs/TiO_2 NTAs exhibited higher PC and PEC performances.

2. Experiments

2.1. Materials

Sodium sulfate (Na_2SO_4), sodium fluoride (NaF), acetone (CH_3COCH_3), absolute ethanol (C_2H_5OH), rhodamine B (RhB), cadmium chloride ($CdCl_2$) and thioacetamide (CH_3CSNH_2) were kindly purchased from Sinopharm Chemical Reagent Co. Ltd. All chemicals used in this study were analytical grade without any further purification. Deionized (DI) water was used throughout our experiments.

2.2. Preparation of CdS NCs/TiO_2 NTAs photoelectrode

Firstly, titanium foils (99.6%, 0.2 mm thickness) were ultrasonically cleaned in acetone and absolute ethanol, followed by rinsing with DI water and drying for 1 h at 80 °C. Typically, anodization process was conducted in a traditional two electrode configurations, in which Ti foils and Pt electrode were served as anode and cathode, respectively. At room temperature (RT), the pre-treated Ti foils (with an efficient electrode area of 2 cm^2) were anodized at 20 V for 2 h in a mixed electrolyte which containing 0.5 wt% NH_4F and 1.0 mol L^{-1} Na_2SO_4. Subsequently, the as-anodized TiO_2 NTAs samples were rinsed with DI water and dried for 24 h at 343 K. Finally, the obtained samples were annealed for 2 h at 723 K in a muffle furnace with a heating rate of 3 °C min^{-1}.

In this study, CdS NCs/TiO_2 NTAs photoanode have been prepared through electrodeposition strategy, in which Pt electrode and TiO_2 NTAs were served as the anode and cathode electrodes, respectively. The electrolyte solution was $CdCl_2$ (0.1 mol L^{-1}) and CH_3CSNH_2 (0.06 mol L^{-1}). Electrodeposited process was performed at 0.8 V for 0.5 h. After electrodeposition, the as-obtained samples were rinsed with DI water and annealed at 623 K for 2 h in a muffle furnace with a heating rate of 3 °C min^{-1}.

2.3. Characterization

The morphologies of samples were observed by using a field emission scanning electron microscope (Quanta 200F). X-ray diffraction (XRD) has been performed on a D8 Advance (Bruker) diffractometer with Cu Kα radiation. The accelerating voltage and applied current were held at 40 kV and 30 mA, respectively. Ultraviolet–visible diffuse reflectance spectroscopy (UV–vis DRS) was recorded on a TU-1901 spectrophotometer equipped with an integrating sphere, in which $BaSO_4$ was used as the reflectance sample. The photoelectrochemical (PECH) measurements were measured on a LK 3200 electrochemical workstation in a three-cell configuration with the as-prepared TiO_2 NTAs, Pt electrode and saturated calomel electrode (SCE) as the photoanode, counter electrode and reference electrode, respectively. Na_2SO_4 solution (0.1 mol L^{-1}) was served as the supporting electrolyte. Meanwhile, a 350 W Xenon arc lamp was served as the simulated solar light source, which was placed 15 cm beside the light source. Photoluminescence (PL) spectra were measured at RT on an FP-6500 fluorescence spectrophotometer (Hitachi, Japan).

2.4. Evaluation of photoelectrocatalysis (PEC) and photocatalysis (PC)

The PEC and PC degradations were carried out in a self-made cylindrical quartz photoreactor, which contained 30 mL solution of Na_2SO_4 (0.1 mol L^{-1}) and RhB (5 mg L^{-1}). Prior to irradiation, CdS NCs/TiO_2 NTAs electrode was vertically fixed in the reactor and then magnetic stirred for 30 min in the dark to establish the equilibrium of adsorption/desorption. Afterwards, 350 W Xenon light was switched on. At given time intervals, the collected samples were filtrated and measured at 553 nm using a T6 UV–vis spectrophotometer. It should be noted that the PEC process was conducted under the same procedure, while a 2 V external potential was applied and controlled by a two-channel output DC power supply (DH1715A-5).

3. Results and discussion

3.1. SEM and TEM analysis

Fig. 1 showed the typical SEM images of the as-prepared bare TiO_2 NTAs and CdS NCs/TiO_2 NTAs photoelectrodes. Clearly, it can be observed that the average inner diameter of bare TiO_2 NTAs was about 94 nm with a wall thickness of about 19 nm (Fig. 1a). However, as shown in Fig. 1B, highly ordered nano-tubular structure could also be observed, which possessed an average inner diameter of around 120 nm and wall thickness of 20 nm. Furthermore, as shown in Fig. 1b, CdS NCs were uniformly deposited onto the surface of the highly oriented TiO_2 NTAs with a uniform size of about 20 nm. In addition, as displayed in Fig. 1c, the shapes and surface structures of CdS NCs/TiO_2 NTAs were further confirmed by TEM and HRTEM. As shown in inset of Fig. 1c, the perfect lattice fringes of 0.352 nm could be clearly observed, which was in accordance with the (101) plane of anatase TiO_2 [11]. Moreover, as seen from the TEM bright field image of CdS NCs/TiO_2 NTAs sample (as shown in inset of Fig. 1c), diffraction spots along with diffraction rings could be obviously observed, revealing the existence of CdS NCs.

3.2. XRD and DRS analysis

XRD patterns of TiO_2 NTAs and CdS NCs/TiO_2 NTAs samples were performed and shown in Fig. 2A. Clearly, as shown in Fig. 2A, all the crystallite phase could be indexed from their corresponding characteristic peaks using the anatase phase (JCPDS No. 21-1272) and Ti metal phase (JCPDS NO. 44-1294) [12], which were marked distinctly with A and T in the XRD patterns, respectively. However, it should be noted that after decoration with CdS NCs, TiO_2 NTAs sample exhibited three additional diffraction peaks located at 26.5°, 43.8° and 51.4°, corresponding to the hexagonal phase (1 1 1), (2 2 0), (3 1 1) of CdS NCs [13]. Thus, it was reasonable that CdS NCs were successfully deposited onto the surface of TiO_2 NTAs.

In order to investigate the light absorption ability of the as-prepared TiO_2 NTAs samples, UV–vis diffuse reflectance spectra (DRS) were recorded. As shown in Fig. 2B, both TiO_2 NTAs samples exhibited typical onset absorption edge at about 390 nm, corresponding to the electronic transition from O^{2-} anti-bonding orbital to the lowest empty orbital of Ti^{4+} ($O2p \rightarrow Ti3d$) [14]. Nevertheless, compared with bare TiO_2 NTAs, the light absorbance edge of CdS NCs/TiO_2 NTAs photoelectrode was significantly red-shifted to visible region with the strongest peak located at 450 nm between

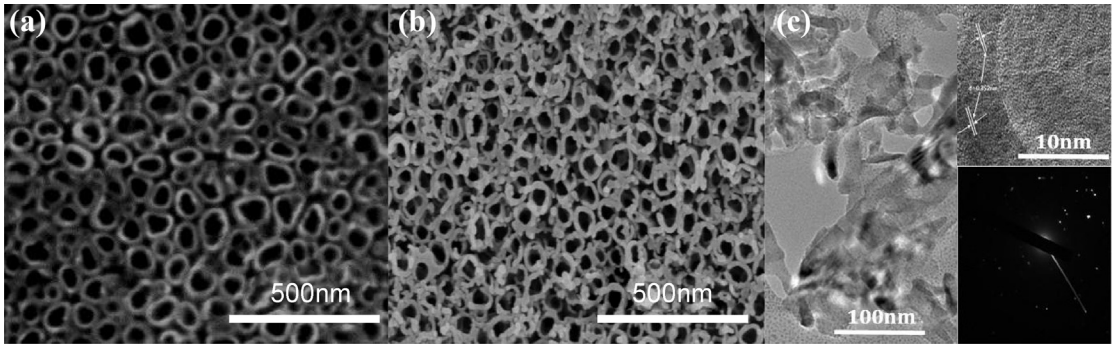

Fig. 1. (a) SEM image of bare TiO_2 NTAs, (b) SEM image of CdS NCs/TiO_2 NTAs and (c) TEM image CdS NCs/TiO_2 NTAs photoelectrode.

400 and 700 nm, which could be attributed to the decoration of CdS NCs, which responsible for improvement of visible light capability of CdS NCs/TiO_2 NTAs. Furthermore, the band gap of TiO_2 NTAs could be calculated through the following Kubelka–Munk equation [15].

$$(\alpha h\nu) = A(h\nu - E_g)^{n/2} \quad (1)$$

where α, ν, E_g, and A are absorption coefficient, light frequency, band gap, and a constant, respectively. Among them, n depends on the characteristics of the transition in a semiconductor, i.e., direct transition ($n = 1$) or indirect transition ($n = 4$). After calculating, the band gap of TiO_2 NTAs and CdS NCs/TiO_2 NTAs were found to be 3.2 eV and 2.75 eV, respectively. Thus, undoubtedly, these results indicated that CdS NCs were indeed deposited onto the surface of TiO_2 NTAs, which was in accordance with the XRD and SEM results. Moreover, we could propose that crystalline CdS was synthesized under mild ambience, and the reaction could be described concisely as followed (Eqs. (2) and (3)):

$$CH_3CSNH_2 + 2H_2O \rightarrow NH_3 + CH_3COOH + H_2S \quad (2)$$

$$CdCl_2 + H_2S \rightarrow CdS + 2HCl \quad (3)$$

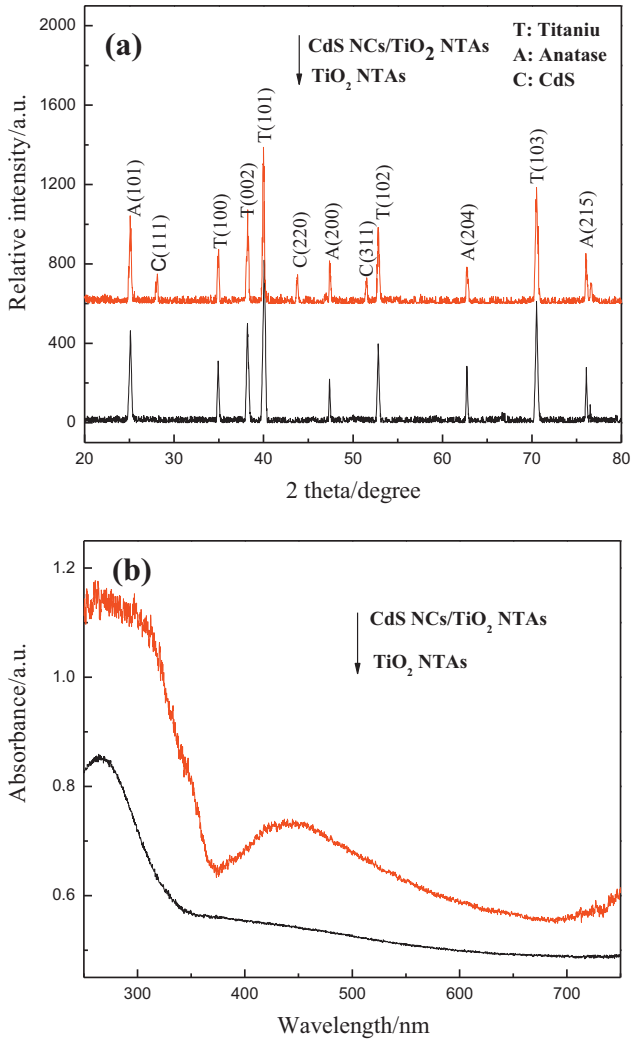

Fig. 2. XRD patterns (a) and DRS spectra (b) of bare TiO_2 NTAs and CdS NCs/TiO_2 NTAs photoelectrodes.

3.3. PECH measurements

Generally, the PEC response has always been considered as an effective parameter to evaluate the PC and PEC performances of TiO_2-based nano-materials. Thus, the transient photocurrent response (PCR) was conducted to access the separation efficiency of photogenerated holes and electrons (h^+/e^-) pairs. As shown in Fig. 3a, as soon as under Xenon lamp irradiation, the photocurrent response generated promptly and increased sharply, while went down to zero as soon as the irradiation of light on the photoanode was stopped, suggesting that the current was completely arose from the activity of the as-prepared TiO_2 NTAs photoelectrode. In addition, the transient photocurrent density of CdS NCs/TiO_2 NTAs (9.62 mA cm^{-2}) was 1.3 times as high as that of bare TiO_2 NTAs (7.37 mA cm^{-2}), indicating the perfect separation efficiency of photogenerated charge carriers of CdS NCs/TiO_2 NTAs.

Meanwhile, the open-circuit potentials (OCP) of both TiO_2 NTAs photoelectrodes were measured to evaluate the generation and recombination of e^-/h^+ pairs. As displayed in Fig. 3b, both TiO_2 NTAs electrodes displayed a distinct OCP. Noticeable, CdS NCs/TiO_2 NTAs performed a higher photovoltage than that of the bare TiO_2 NTAs. When the Xenon light was switched on, the OCP of CdS NCs/TiO_2 NTAs shifted promptly and reached instantaneously to -0.253 V cm^{-2}, while the OCP of bare TiO_2 NTAs increased gradually to -0.232 V cm^{-2}. When the light was off, the OCP of CdS NCs/TiO_2 NTAs decreased more quickly than that of TiO_2 NTAs electrode. Thus, it can be suggested that CdS NCs/TiO_2 NTAs electrodes exhibited a more sensitive and effective separation of photogeneratd charge carriers, which was consistent with the photocurrent property.

3.4. PEC and PC performances

Rhodamine B (RhB) has been widely employed as a dye, especially for textile and industrial dyes. Recently, it was found to be potentially toxic and carcinogenic [16]. Thus, RhB molecules

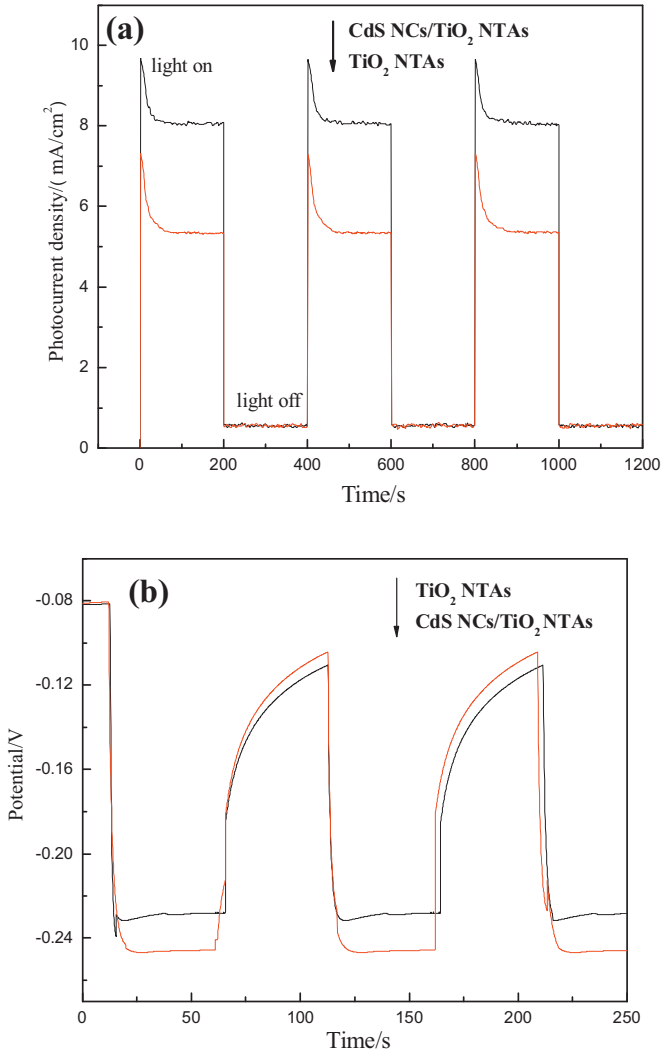

Fig. 3. Photocurrent response (a) and open-circuit photovoltage (b) of bare TiO_2 NTAs and CdS NCs/TiO_2 NTAs photoelectrodes.

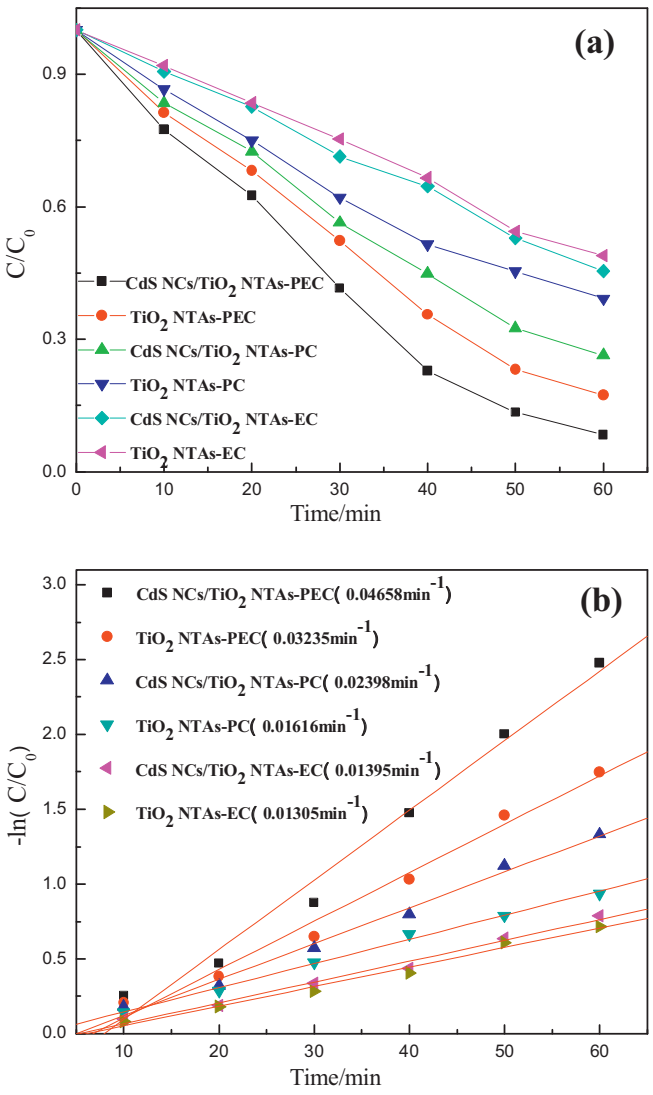

Fig. 4. PC, EC and PEC degradation rates (a) and evolution curves (b) of RhB solution on as-prepared bare TiO_2 NTAs and CdS NCs/TiO_2 NTAs photoelectrodes (the corresponding degradation rate constants were listed in the parentheses).

were often chosen as a representative pollutant to evaluate the PC performance of the as-synthesized catalysts. Thus, in this study, the degradation of RhB was used to evaluate the PEC and PC performances of the as-constructed CdS NCs/TiO_2 NTAs photoelectrodes. In addition, the EC process was also measured as a reference. Compared with PC and PEC efficiencies, the removal of direct photolysis or adsorption in dark of RhB (<3%) was so low that it could be neglected. As seen from Fig. 4a, the PC, PEC and EC performances of TiO_2 NTAs were greatly improved by decoration with CdS NCs, which was in good agreement with DRS and PECH results. However, compared with the PEC and PC efficiencies, EC process of both of TiO_2 NTAs samples exhibited lower degradation efficiency, indicating that external potential (2 V in our case) could significantly increase the PC performance, which was mainly ascribed to the following aspect that external potential improved the charge transfer and separation properties. Furthermore, the degradation efficiencies of both TiO_2 NTAs samples can be ranged in the following orders: CdS NCs/TiO_2 NTAs-PEC > TiO_2 NTAs-PEC > CdS NCs/TiO_2 NTAs-PC > TiO_2 NTAs-PC > CdS NCs/TiO_2 NTAs-EC > TiO_2 NTAs-EC. That was, CdS NCs/TiO_2 NTAs exhibited highest PEC performance for the degradation of RhB than that of others, for which 91.6% of RhB could be degraded within 60 min irradiation, which was attributed to the following two aspects. (1) External potential facilitated the charge transfer and mobility, leading to a higher separation efficiency of photogenerated charge carriers thereby inducing a higher PEC degradation efficiency. (2) TiO_2 NTAs decoration with CdS NCs significantly improved the visible light absorption capacity, which could induce more photons to participate in the PC reaction, resulting in a higher PC efficiency.

Clearly, as shown in Fig. 4b, the degradation rate of RhB fitted well with the pseudo-first-order kinetics function according to the Langmuir–Hinshelwood (L-H) model within 60 min [17]. It should be noted that CdS NCs/TiO_2 NTAs exhibited superior PC, EC and PEC performances than that of bare TiO_2 NTAs sample under the paralleled conditions. Furthermore, it can be induced that external potential further improved their PC activities. Noticeable, CdS NCs/TiO_2 NTAs photoanode displayed the highest PEC activity with the rate constant of 0.04658 min^{-1} under simulated solar light irradiation. The enhanced PEC performance could be attributed to the intense visible light absorbance, and efficient mobility and separation of photogenerated charge carriers.

The formation rate of •OH radicals at photo-illuminated catalyst/water interface was detected by PL technique using terephthalic acid (TA) as a probe molecule, which could react readily react

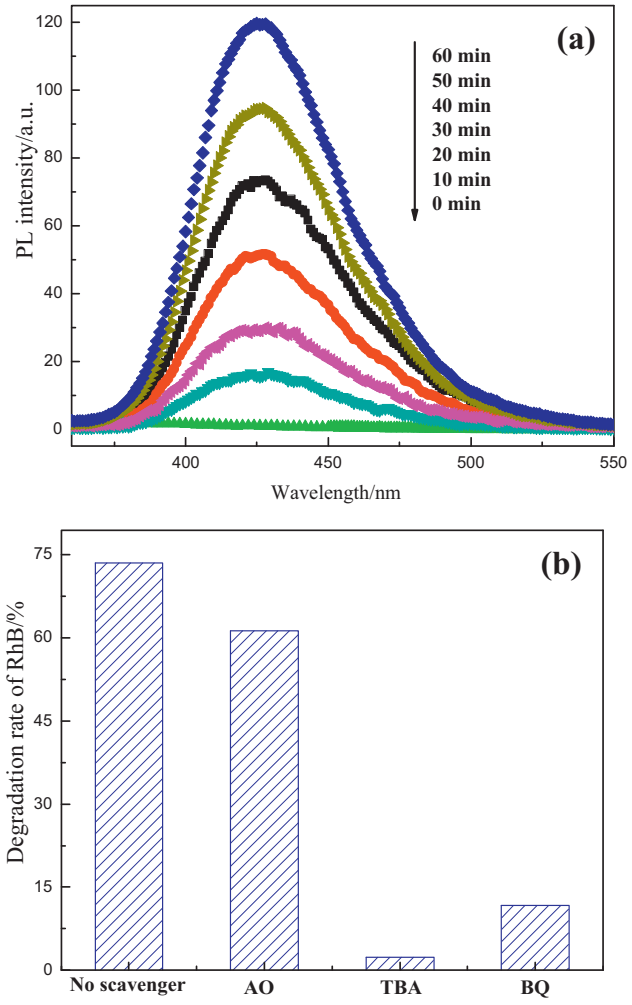

Fig. 5. (a) PL spectral changes with simulated solar light irradiation time on the CdS NCs/TiO_2 NTAs sample and (b) the photocatalytic degradation of RhB with or without different scavengers (10 mM).

with the generated •OH radicals to form highly fluorescent products, 2-hydroxyterephthalia acid (TAOH) [18]. Fig. 5a showed the evolution of PL intensity of TAOH produced from 0.5 mM TA solution under simulated solar light irradiation with irradiation time in the presence of CdS NCs/TiO_2 NTAs. Clearly, as shown in Fig. 5a, a gradual increase in the PL intensity at about 425 nm was observed with time for CdS NCs/TiO_2 NTAs sample. However, no PL signal was observed in the absence of simulated solar light irradiation.

Furthermore, in order to distinguish the contribution of each reactive species to the PC degradation of RhB, several scavengers were conducted and shown in Fig. 5b. Tert butyl alcohol (TBA) was added into the solution to scavenge •OH radicals [19], benzoquinone (BQ) was selected as scavenger $^{\bullet}O_2^-$ [20], and ammonium oxalate (AO) was used as a hole scavengers [21]. On the contrary, the PC degradation of RhB decreased with the addition of scavengers. In addition, it should be noted that the PC degradation of RhB was completely restricted, demonstrating that •OH radicals were mainly responsible for the PC degradation of RhB. However, the formed h^+ can be slightly hindered in the presence of AO, indicating that the contribution of h^+ was very limited. Similarly, when the generated $^{\bullet}O_2^-$ was suppressed by BQ, the PC degradation was greatly decreased from 73.6 to 11.7%. Therefore, it can be induced that each reactive species played important role in the PC reactions.

Based on the above analysis, the reason that CdS NCs/TiO_2 NTAs exhibited high visible light PC performance can be explained using the scheme shown in Fig. 6. Pure TiO_2 NTAs sample exhibited low PC efficiency due to its wide band gap. However, after decoration with CdS NCs, electrons can be easily excited from the valence band to conduction band of CdS nano-semiconductor which possessed narrower band gap (Eq. (4)). Subsequently, the electrons could be jumped to the conduction band of TiO_2 due to its lower Fermi level. After that, the departed electrons could be migrated to the surface of TiO_2. Finally, the separated electrons could react with the adsorbed O_2 to form the active species of •OH radicals (Eqs. (6) and (7)), which responsible for the mineralization of organic pollutants (Eq. (8)). Moreover, the residual holes in the valence band of CdS NCs could also react with H_2O to form the •OH radicals (Eq. (5)). The detail reaction could be described as followed:

$$CdS + h\nu \rightarrow e_{CB}^- + h_{VB}^+ \quad (4)$$

$$h_{VB}^+ + H_2O_{(ads)} \rightarrow {}^{\bullet}OH + H^+ \quad (5)$$

$$e_{CB}^- + O_2 \rightarrow {}^{\bullet}O_2^- \quad (6)$$

$$^{\bullet}O_2^- + 2H^+ + 2e_{CB}^- \rightarrow {}^{\bullet}OH + OH^- \quad (7)$$

$$^{\bullet}OH + \text{Organics} \rightarrow \cdots \rightarrow CO_2 + H_2O \quad (8)$$

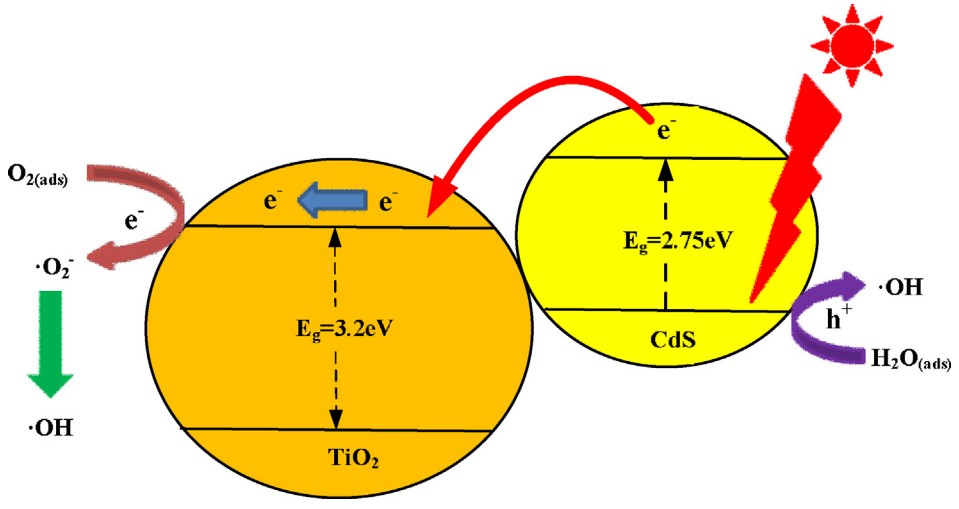

Fig. 6. Scheme of visible light photocatalytic mechanism of CdS NCs/TiO_2 NTAs photoelectrode.

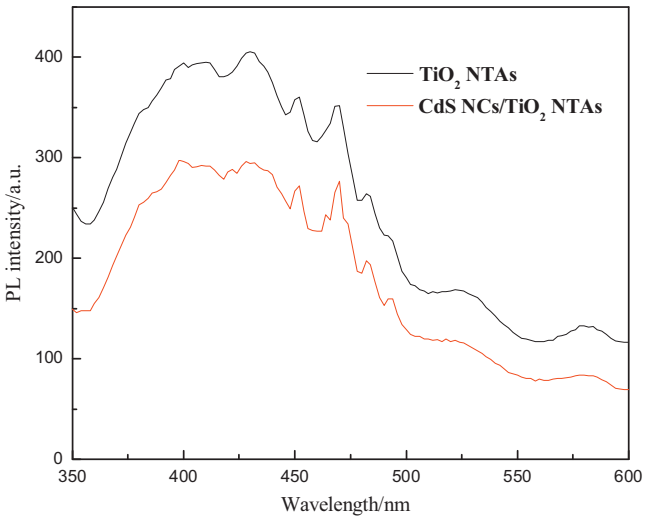

Fig. 7. Comparison of PL spectra of bare TiO_2 NTA and CdS NCs/TiO_2 NTAs photoelectrodes.

Usually, photoluminescence (PL) spectra have been widely employed to investigate surface processes involving the efficiency of charge carriers trapping, immigration and transfer of photogenerated electrons and holes [22]. Generally speaking, the band–band PL spectrum directly reflects the separation of photogenerated charge carriers. Meanwhile, strong band–band PL signal corresponds to the high recombination efficiency of photogenerated charge carriers, thereby resulting in a low PC efficiency. The excitonic PL spectra can disclose some significant information such as surface defects, oxygen vacancies and surface states, which could strongly influence the PC reactions. Therefore, to confirm the proposition, PL spectra of TiO_2 NTAs and CdS NCs/TiO_2 NTAs were measured at RT in the wavelength range of 350–600 nm (Fig. 7). It should be noted that both of TiO_2 NTA samples exhibited similar shape of PL spectra. The broad and strong PL signals located at 397 and 410 nm were attributed to the band–band PL phenomenon with the energy of light approximately equal to the band gap energy of anatase. The other four peaks at 451, 468, 483 and 492 nm were assigned to the excitonic PL [23]. Furthermore, the PL intensity of CdS NCs/TiO_2 NTAs exhibited a obviously decrease compared with bare TiO_2 NTAs, suggesting that CdS NCs/TiO_2 NTAs displayed a lower recombination rate of photogenerated electrons and holes under simulated solar light irradiation, which was ascribed to the aspect that the electrons were excited from the valence band to the conduction band of CdS and then transferred to TiO_2 NTAs, which prevented the direct recombination of electrons and holes.

4. Conclusions

In summary, CdS nano-crystallites decorated TiO_2 nano-tubes arrays (CdS NCs/TiO_2 NTAs) photoelectrodes were prepared through anodization, followed by electrodeposition strategy. It can be induced that decoration with hexagonal CdS NCs with uniform spherical sizes of 20 nm was responsible for the improvement of visible light harvesting range from 400 to 700 nm, high transient photoinduced current of 9.62 $mA{\cdot}cm^{-2}$ and open-circuit photovoltage of -0.253 $mV{\cdot}cm^{-2}$ of highly ordered TiO_2 NTAs, as well as efficient separation of photogenerated electrons–holes pairs and production of ·OH radicals, which have been confirmed by light absorption property, photocurrent response, open circuit photovoltage and PL technique analysis, respectively. Furthermore, it should be noted that the PEC degradation of RhB fitted well with the pseudo-first-order kinetics function and ·OH radicals was the dominated reactive species. The enhanced visible light PC mechanism was mainly attributed to the decoration of CdS NCs, which could not only induce the visible light harvesting, but also provide superior pathway for the transfer and separation of charge carriers. The CdS NCs/TiO_2 NTA photoanode are also of great interest for sensors, solar cells and water splitting.

Acknowledgments

This work was supported by National Natural Science Foundation of China for Youth (21106035) and Youth Scholar Backbone Supporting Plan Project for general colleges and universities of Heilongjiang province (1151G034).

References

[1] M. Grätzel, Photoelectrochemical cells, Nature 414 (2001) 338.
[2] M. Andersson, L. Osterlund, S. Ljungstrom, A. Palmqvist, Preparation of nanosize anatase and rutile TiO_2 by hydrothermal treatment of micro-emulsions and their activity for photocatalytic wet oxidation of phenol, Journal of Physical Chemistry B 106 (2002) 10674.
[3] E.Y. Bae, W.Y. Choi, Highly enhanced photoreductive degradation of perchlorinated compounds on dye-sensitized metal/TiO_2 under visible light, Environmental Science and Technology 37 (2003) 147.
[4] M.I. Litter, Heterogeneous photocatalysis transition metal ions in photocatalytic systems, Applied Catalysis B: Environmental 23 (1999) 89.
[5] K. Shin, S. Seok, S.H. Im, J.H. Park, CdS or CdSe decorated TiO_2 nanotube arrays from spray pyrolysis deposition: use in photoelectrochemical cells, Chemical Communications 46 (2010) 2385.
[6] Y. Hou, X.Y. Li, X.J. Zou, X. Quan, G.H. Chen, Photoeletrocatalytic activity of a Cu_2O-loaded self-organized highly oriented TiO_2 nanotube array electrode for 4-chlorophenol degradation, Environmental Science and Technology 43 (2009) 858.
[7] Y. Xie, S.H. Yoo, C. Chen, S.O. Cho, Ag_2S quantum dots-sensitized TiO_2 nanotube array photoelectrodes, Materials Science and Engineering B 177 (2012) 106.
[8] L. Zhu, Z.D. Meng, C.K. Park, T. Ghosh, W.C. Oh, Characterization and relative sonocatalytic efficiencies of a new MWCNT and CdS modified TiO_2 catalysts and their application in the sonocatalytic degradation of rhodamine B, Ultrasonics Sonochemistry 1 (2013) 478.
[9] J.J. Tian, Q.F. Zhang, L.L. Zhang, R. Gao, L.F. Shen, S.G. Zhang, X.H. Qu, G.Z. Cao, ZnO/TiO_2 nanocable structured photoelectrodes for CdS/CdSe quantum dot co-sensitized solar cells, Nanoscale 3 (2013) 936.
[10] P.K. Santra, P.V. Kamat, Tandem-layered quantum dot solar cells: tuning the photovoltaic response with luminescent ternary cadmium chalcogenides, Journal of the American Chemical Society 2 (2013) 877.
[11] W. Zhou, F.F. Sun, K. Pan, G.H. Tian, B.J. Jiang, Z.Y. Ren, C.G. Tian, H.G. Fu, Well-ordered large-pore mesoporous anatase TiO_2 with remarkably high thermal stability and improved crystallinity: preparation, characterization, and photocatalytic performance, Advanced Materials 21 (2011) 1922.
[12] J.G. Yu, G.P. Dai, B. Cheng, Effect of crystallization methods on morphology and photocatalytic activity of anodized TiO_2 nanotube array films, Journal of Physical Chemistry C 114 (2010) 19378.
[13] R.S. Mane, C.D. Lokhande, Studies on chemically deposited cadmium sulphoselenide (CdSSe) films, Thin Solid Films 304 (1997) 56.
[14] X.W. Cheng, X.J. Yu, Z.P. Xing, Characterization and mechanism analysis of Mo-N-co-doped TiO_2 nano-photocatalyst and its enhanced visible activity, Journal of Colloid and Interface Science 372 (2012) 1.
[15] F. Spadavecchia, C. Cappelletti, S. Ardizzone, C.L. Bianchi, S. Cappelli, C. Oliva, P. Scardi, M. Leoni, P. Fermo, Solar photoactivity of nano-N-TiO_2 from tertiary amine: role of defects and paramagnetic species, Applied Catalysis B: Environmental 96 (2010) 314.
[16] J.C. Zhao, T.X. Wu, K.Q. Wu, K. Oikawa, H. Hidaka, N. Serpone, Photoassisted degradation of dye pollutants. 3. Degradation of the cationic dye rhodamine B in aqueous anionic surfactant/TiO_2 dispersions under visible light irradiation: evidence for the need of substrate adsorption on TiO_2 particles, Environmental Science and Technology 32 (1998) 2394.
[17] M.R. Hoffmann, S.T. Martin, W.Y. Choi, D.W. Bahnemann, Environmental applications of semiconductor photocatalysis, Chemical Reviews 95 (1995) 69.
[18] Q. Xiao, Z.C. Si, J. Zhang, C. Xiao, X.K. Tan, Photoinduced hydroxyl radical and photocatalytic activity of samarium-doped TiO_2 nanocrystalline, Journal of Hazardous Materials 150 (2008) 62.
[19] Y.M. Lin, D.Z. Li, J.H. Hu, G.C. Xiao, J.X. Wang, W.J. Li, X.Z. Fu, Highly efficient photocatalytic degradation of organic pollutants by PANI-modified TiO_2 composite, Journal of Physical Chemistry C 116 (2012) 5764.
[20] L.Q. Ye, J.Y. Liu, C.Q. Gong, L.H. Tian, T.Y. Peng, L. Zan, Two different roles of metallic Ag on Ag/AgX/BiOX (X = Cl, Br) visible light photocatalysts: surface plasmon resonance and Z-scheme bridge, ACS Catalysis 2 (2012) 1677.

[21] W.J. Li, D.Z. Li, W.J. Zhang, Y. Hu, Y.H. He, X.Z. Fu, Microwave synthesis of $Zn_xCd_{1-x}S$ nanorods and their photocatalytic activity under visible light, Journal of Physical Chemistry C 114 (2010) 2154.
[22] J.G. Yu, H.G. Yu, B. Cheng, X.J. Zhao, J.C. Yu, W.K. Ho, The effect of calcination temperature on the surface microstructure and photocatalytic activity of TiO_2 thin films prepared by liquid phase deposition, Journal of Physical Chemistry B 107 (2003) 13871.
[23] L.Q. Jing, X.J. Sun, W.M. Cai, Z.L. Xu, Y.G. Du, H.G. Fu, The preparation and characterization of nanoparticle TiO_2/Ti films and their photocatalytic activity, Journal of Physics and Chemistry of Solids 64 (2003) 615.